DTU Library

H∞ Current Damping Control of DFIG based Wind Farm for Sub-Synchronous Control Interaction Mitigation

Wang, Yun; Wu, Qiuwei; Yang, Rong; Tao, Guoqing ; Liu, Zhaoxi

Published in:
International Journal of Electrical Power & Energy Systems

Link to article, DOI:
10.1016/j.ijepes.2017.12.003

Publication date:
2018

Document Version
Peer reviewed version

H_∞ Current Damping Control of DFIG based Wind Farm for Sub-Synchronous Control Interaction Mitigation

Yun Wang[a], Qiuwei Wu[b*], Rong Yang[a*], Guoqing Tao[a], Zhaoxi Liu[b]

[a] College of Mechatronics and Control Engineering (Shenzhen University), Nanhai Ave 3688, Shenzhen, PR China

[b] Centre for Electric Power and Energy (CEE), Department of Electrical Engineering, Technical University of Denmark (DTU), Elektrovej 325, Kgs. Lyngby, DK-2800, Denmark

Abstract

This paper proposes an H_∞ damping controller for the doubly-fed induction generator (DFIG) based wind farm (WF) to mitigate sub-synchronous control interactions (SSCI) with series capacitor compensated lines. A multi-input multi-output (MIMO) uncertain state-space model is developed to reflect the main SSCI characteristics considering the uncertainties of wind speed, series compensation (SC) levels and system parameters. The SSCI is analyzed using the eigenvalue analysis of the uncertain system model. In order to damp the SSCI between the WF and series capacitor compensated lines under uncertainties, an H_∞ damping controller is designed for the rotor side converter (RSC). The weighting functions are designed to meet the mitigation requirements of sub-synchronous oscillation currents and output power. The robust stability (RS) and robust performance (RP) of the system are validated by the μ analysis. The performance of the H_∞ damping controller is demonstrated by time domain simulations of a 90 MW wind farm model with different wind speed, and SC levels. The case study with 6 m/s wind speed and 70% SC level shows superior performance of the H_∞ damping controller.

Keywords: Doubly-fed induction generator (DFIG), robust control, series compensation, sub-synchronous control interaction (SSCI), wind farm.

*Corresponding author:
Email address: qw@elektro.dtu.dk , ryang@szu.edu.cn

Nomenclature

a. Subscripts

L, T	Transmission line, transformer.
abc	Stationary A, B, and C phases.
d, *q*	Synchronous *d*- and *q*-axis.
g, *sc*	GSC, series capacitor.
m, *l*	Mutual, leakage.
s, *r*	Stator, rotor.
*	Reference value for controller (Superscript).

b. Parameters and variables

C, L	Capacitor, inductance.
Dt, *Dtg*	Damping coefficients of turbine and generator.
Hg, *Ht*	Inertia constants for generator and turbine.
Ktg, *Kp*, *Ki*	Shaft stiffness, parameters of PI controller.
Ksc	Series compensated level.
LLT	Submission of *LL* and *LT*.
P, Q	Active, reactive power.
R, X	Resistance, reactance.
S, slip	Laplace coefficient, DFIG slip ratio.
Udc, *Te*	Converter DC voltage, electromagnetic torque.
f, i, u,ω	Frequency, currents, voltage and angular speed.
fn	Electrical resonance frequency.
ωe, *ωt*	Electrical, mechanical angular speeds.
ω_B, *ωslip*	Nominal (100π), slip angular speeds.

1. Introduction

Sub-synchronous resonance (SSR) of the wind farm (WF) is a phenomenon that wind turbines (WTs) exchange energy with the electric network at one or more natural frequencies below the fundamental frequency of the power system [1]. The SSR may occur when the WF is connected to alternating-current (AC) transmission lines compensated with series-capacitors [2]-[4]. According to different components of WTs interacting with series compensation (SC), the SSR of the WF can be divided into three types [5]-[7]: induction generator effect (IGE), torsional interaction (TI), and sub-synchronous control interaction (SSCI). The excitation component of each type is listed in Table I. The analyses in [4]-[6] show that the TI is not a concern for the WF because a very high level of SC is required to excite the low frequency torsional modes of the TI, which rarely happens. The IGE and SSCI are the two main SSR types in the WF.

The modeling, analysis and mitigation control of SSR on doubly-fed induction generator (DFIG) based WT have been widely studied in the last decade [5]-[13]. These studies show that the DFIG based WF is very susceptible to the SSCI, which can build up within hundreds of milliseconds or less. Therefore, the SSCI can cause damages very fast, i.e., leading to excessive currents both at the WT level and point of common coupling (PCC), and creating significant over-voltages at the utility level before the relays detect [3]. Such events have been reported in the Electric Reliability Council of Texas (ERCOT) system and other places.

TABLE I

Comparison of IGE, TI and SSCI

<table>
<tr><th>Type</th><th colspan="2">Excitation component</th></tr>
<tr><td>IGE</td><td rowspan="3">Series-compensated electrical network</td><td>Induction generator</td></tr>
<tr><td>TI</td><td>Mechanical drive-train</td></tr>
<tr><td>SSCI</td><td>Power electronics device with control system</td></tr>
</table>

With the IEEE first benchmark model (FBM) or more complicated system with multiple SC transmission lines [2]-[4], the system frequency characteristic under the SSCI were studied, showing that the oscillation frequencies due to the SSCI vary with different topologies, wind speed, grid parameters, etc. [5]-[14]. However, these models are all based on the certain parameters of DFIG WF and transmission lines. The uncertainties of system reactance and resistance are not considered, which can greatly influence the sub-synchronous oscillation of the system as [6]-[7] indicate.

Using the frequency-scan approach, electro-magnetic transient (EMT) simulation and eigenvalue analysis methods, the factors affecting the SSCI on DFIG based WF were studied [5]-[14], showing the wind speed, SC level and control parameters are the most important factors of the SSCI phenomenon of the DFIG base WF. With the wind speed reducing or SC level increasing, the absolute value of equivalent rotor resistance may exceed the sum of stator and network resistance, leading the generation system destabilized, which is called the induction generator effect (IGE) [8]-[10]. Besides the IGE, the generation control system of the DFIG also interacts with transmission lines, which is called sub-synchronous control interaction (SSCI) [11]-[14]. The modal analyses in

[12]-[13] indicate, with the control gains of grid side converter (GSC) and rotor side converter (RSC) increasing, the sub-synchronous mode of the DFIG is pushed to the right half plane, resulting in the DFIG instability. The SSCI analyses also indicate that the impact of the GSC controller on the SSCI of DFIG is not as much as the RSC controller and the most important factor of the control system is the rotor current control gains [12], [13], [15].

The previous studies indicate that, when a SSR phenomenon occurs, the sub-synchronous oscillation of DFIG stator and rotor currents develop very fast, leading to current oscillation both at the WT level and point of connection (POC), and creating significant over-voltages at the utility level before the relays detect [3], [8]-[13]. By adding flexible ac transmission systems (FACTS) or improving damping of the GSC and RSC control system, the SSCI can be efficiently mitigated [16], [17], [20], [21]. Although the oscillation of the GSC output currents can be mitigated by the GSC current damping control, the influence of the GSC on DFIG SSR phenomenon and the SSCI mitigation performance of the whole DFIG system through the GSC controller is limited [12], [15], [17]. The reason is because the power flow ratio of the stator side and the rotor side or GSC side is approximately (1-slip)/slip. The GSC maximum capacity is about 30% of the DFIG nominal capacity [18], [19], and the sub-synchronous oscillation of the stator currents cannot be sufficiently mitigated through the GSC control. By the rotor current damping control of the RSC, the oscillation of stator currents can be well mitigated. Because the stator current is controlled for the output power of the WT, current damping control through the RSC can realized efficient damping performance of the DFIG.

Several current damping control methods through the RSC have been proposed. Decreasing the bandwidth of the rotor current controller and adding SSCI damping filter paralleled with the RSC current controller are used to decrease currents oscillation and improve the stability of the DFIG [20]. However, this will deteriorate the dynamic performance of the control system, and the SSCI damping performance under very low wind speed, high SC level, and uncertain system conditions are not guaranteed. Reference [16] proposed a gain-scheduling adaptive control (GSA) to compensate the control performance both with wind speed and SC level changes. However, the GSA control design is based on the certain DFIG model, and the system parameter uncertainty is not considered. Reference [21] proposed a two-degree-of-freedom control (DOF) with a damping control loop paralleled with the rotor currents loop. Reference [29] proposed a linear-quadratic-gaussian control to mitigate the SSCI of DFIG, and the system uncertainty is regarded as error dynamics. Reference [30] used the concise form of a second-order band-stop filter efficiently tuned to mitigate SSR. Reference [31] developed an optimal control-design method for TI between turbo-generators and the series compensated grid. However, most of the methods are based on the certain state-space controlled model, and the possible system uncertainties such as the SC level, line reactance and wind speed are not fully considered. Although they have been efficiently tuned under nominal or certain conditions, the stability cannot be guaranteed under all possible operating conditions. In addition, how to achieve a better SSCI damping performance without sacrificing the control bandwidth needs to be further studied.

The H_∞ robust control has been successfully used in many electrical control fields such as the control of voltage source inverter (VSI) [22], dynamic voltage restorer (DVR) [23], and uninterruptible power supplies [24], DFIG harmonic control [25], etc. As an advanced control method, the system under the H_∞ control is uncertain and has a multi-input multi-output (MIMO) structure. These studies show the most important advantage of the H_∞ controller is the good robustness for uncertain systems. Although the optimal solution of the $H\infty$ norm does not focus on the best performance with the nominal system and the controller structure can be more complex, by introducing the H_∞ norm solution, the H_∞ controller can guarantee required control performance and stability with all uncertain cases [26]-[27]. The system robust stability (RS) and robust performance (RP) can be guaranteed to constrain all the possibilities of the uncertain system into a bound by the μ analysis. Because the wind speed, SC level, and DFIG and transmission line parameters are randomly changed within a range or difficult to obtain the accurate value, the H_∞ robust control is more suitable for the SSCI damping control under uncertain cases.

This paper firstly proposes an H_∞ robust control scheme to mitigate the SSCI of the DFIG based WT with the series capacitor compensated line. The contributions of this paper are summarized as follows: 1) a 6th order uncertain state-space model is established for sub-synchronous resonance (SSR) studies of DFIG with the series capacitor compensated line system. 2) Besides the change of wind speed and SC level, the influence of the system reactance parameter on the RSC current control performance is also considered in the SSR analysis. 3) The proposed H_∞ control strategy can ensure the system stability in the whole range of the SC level ($0 \le K_{SC} \le 1$), wind speed (i.e., $-0.3 \le slip \le 0.3$) and the system reactance uncertainty including DFIG and grid line reactance (i.e., $\pm 50\%$), without sacrificing the controller bandwidth of rotor currents. 4) Both the robust stability and robust performance of the SSR damping current controller are validated by μ-analysis.

This paper is organized as follows. Section 2 describes the uncertain model with the state-space representation, analyzes the SSCI by the eigenvalue analysis. In Section 3, the H_∞ damping controller is designed, the tuning of the controller parameters is given, and the robustness is validated by the structured singular value μ. In Section 4, case studies are presented with time-domain simulations, followed by conclusions.

2. Uncertain modeling and SSCI analysis

The IEEE FBM is commonly used for WF SSR studies [5]-[14], [16]-[21]. The FBM is developed with the minimum sophistication needed to obtain useful SSR results and machine characteristics generally obtainable [2]. As shown in Fig. 1, the WF is aggregated as an equivalent WT, and the grid line is simplified as reactance and series capacitor.

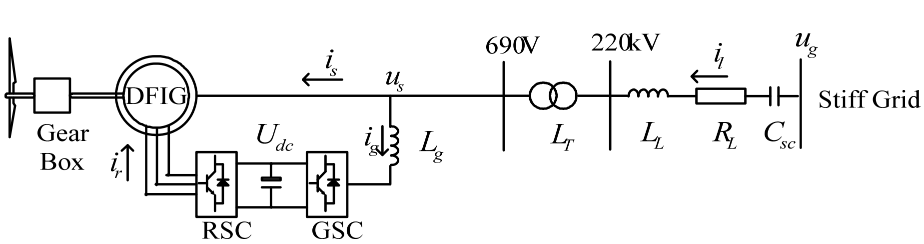

Fig. 1. FBM study diagram with aggregated DFIG based WF.

Because the network is non-ideal with different structures, different network models are usually transformed to an equivalent RLC transmission line to the stiff grid. The impact of the grid characteristics on the SSR of wind farms can be reflected by the series compensation level and grid reactance. In this paper a 1.5 MW DFIG based WT model is scaled up to represent a 90 MW WF. All DFIG variables are marked in the motor direction, and the variables are listed in the Nomenclature.

The WT model consists of the DFIG, the aerodynamic model, the mechanical drive-train model, the back-to-back voltage-source converters, etc. [12]-[13], [18]-[19]. The DFIG control system includes the RSC and GSC parts. The control system adopts vector control method with outer power closed-loop for RSC and DC voltage closed-loop for GSC. The output power loop reference is obtained by the maximum power point tracking (MPPT) technique. Both the RSC and GSC have inner currents closed-loop and phase-locked loop (PLL). The WT model includes a 4th DFIG model, a series compensated network model, the DC Link Model and the mechanical model.

2.1. Uncertain State-space Model of RSC Currents Control

The outer power/speed controller of the RSC adopts conventional proportion integral (PI) regulators. The rotor currents are controlled in the synchronously rotating *dq* frame oriented by the stator voltage. The transmission line reactance is equivalent to the stator side. Because the power flow ratio of the stator and the rotor is approximately (1-*slip*) / *slip* [18][19], neglecting the power loss of the converters, L_{LT} and R_L can be converted from the grid side to the stator side as $L_{LT}' = L_{LT} / (1- slip)$ and $R_L' = R_L / (1- slip)$ approximately. The wind speed, SC level and system reactance are considered as uncertain factors which greatly influence the SSCI of DFIG based WT. The uncertainty of wind speed is reflected as the change of *slip*. The speed operating range of the DFIG is usually $-0.3 \le slip \le 0.3$. The uncertainty of the system reactance parameter is reflected as the change of $L_{LT} = L_T + L_L$. The uncertainty of the series capacitor is reflected as the SC level. The SC level is defined as $K_{SC} = 1/(L_{\omega B}^2 C_{sc} L_{LT})$, and its range is $0 \le K_{SC} \le 1$. The uncertainties are listed in Table II.

Table II

Uncertainty ranges of system parameters

Element	Uncertain range
slip	$\delta_1 = [-0.3, 0.3]$
R_L	$\delta_2 = \pm 50\%$
$L_{LT,L,T}$	$\delta_3 = \pm 50\%$
K_{sc}	$\delta_4 = [0, 1]$

Based on the WT model, the uncertain state-space model for the H_∞ currents controller is developed as (1), (2) and (3), and marked as $G\ (A, B_1, B_2, C)$. The state-space variable vector consists of stator currents, rotor currents and series capacitor voltage, marked as $\boldsymbol{x}=[i_{sd}, i_{sq}, i_{rd}, i_{rq}, u_{scd}, u_{scq}]$. The DFIG is controlled by the RSC. Therefore, $\boldsymbol{u}=[u_{rd}, u_{rq}]$ is the input vector and $\boldsymbol{y}=[i_{rd}, i_{rq}]$ is the output vector. Because stator and rotor currents are coupled with each other, $[i_{sd}, i_{sq}]$ can be indirectly controlled by $\boldsymbol{u}$. Thus $[i_{sd}, i_{sq}]$ and $[i_{rd}, i_{rq}]$ are the state variable vectors. Because $[u_{scd}, u_{scq}]$ is decided by the series capacitor currents as well as the transmission line currents (equal to i_s+i_g) shown in Fig. 1, $[u_{scd}, u_{scq}]$ can also be indirectly controlled by $\boldsymbol{u}$ and considered as the state variable vector. For the RSC, $\boldsymbol{d}=[u_{sd}, u_{sq}]$ is uncontrollable, but can influence $[i_{sd}, i_{sq}]$ directly, and then influence $[i_{rd}, i_{rq}]$ and the transmission line currents indirectly. Therefore, it is considered as a disturbance input vector, independent from the controlled model. $\boldsymbol{u}=[u_{rd}, u_{rq}]$ is adjusted by the RSC controller K.

$$\begin{cases} \dot{\boldsymbol{x}} = A\boldsymbol{x} + [B_1, B_2][\boldsymbol{u},\boldsymbol{d}]^T \\ \boldsymbol{y} = C\boldsymbol{x} + D\boldsymbol{u} \end{cases} \tag{1}$$

$$A = \frac{\omega_B}{L_m^2 - L_r(L_s+L_{LT}')} \begin{bmatrix} L_r(R_s+R_l') & L_m^2\omega_{slip}-(L_s+L_{LT}')L_r\omega_s & -L_mR_r & -L_mL_r\omega_r & L_r & 0 \\ (L_s+L_{LT}')L_r\omega_s-L_m^2\omega_{slip} & L_r(R_s+R_l') & L_mL_r\omega_r & -L_mR_r & 0 & L_r \\ -L_m(R_s+R_l') & (L_s+L_{LT}')L_m\omega_r & (L_s+L_{LT}')R_r & L_m^2\omega_s-(L_s+L_{LT}')L_r\omega_{slip} & -L_m & 0 \\ -(L_s+L_{LT}')L_m\omega_r & -L_m(R_s+R_l') & (L_s+L_{LT}')L_r\omega_{slip}-L_m^2\omega_s & (L_s+L_{LT}')R_r & 0 & -L_m \\ \frac{L_m^2-(L_s+L_{LT}')L_r}{\omega_B C_{sc}(1\text{-}slip)} & 0 & 0 & 0 & 0 & L_m^2-(L_s+L_{LT}')L_r \\ 0 & \frac{L_m^2-(L_s+L_{LT}')L_r}{\omega_B C_{sc}(1\text{-}slip)} & 0 & 0 & (L_s+L_{LT}')L_r-L_m^2 & 0 \end{bmatrix} \tag{2}$$

$$B_1 = \frac{\omega_B}{L_m^2 - L_r(L_s+L_{LT}')} \begin{bmatrix} L_m & 0 & -(L_s+L_{LT}') & 0 & 0 & 0 \\ 0 & L_m & 0 & -(L_s+L_{LT}') & 0 & 0 \end{bmatrix}^T, \quad B_2 = \frac{\omega_B}{L_m^2 - L_r(L_s+L_{LT}')} \begin{bmatrix} -L_r & 0 & L_m & 0 & 0 & 0 \\ 0 & -L_r & 0 & L_m & 0 & 0 \end{bmatrix}^T, \tag{3}$$

$$C = \begin{bmatrix} 0 & 0 & 1 & 0 & 0 & 0 \\ 0 & 0 & 0 & 1 & 0 & 0 \end{bmatrix}, \quad D = 0$$

2.2. The SSCI Analysis of RSC Currents Controlled System

Fig. 2 shows the frequency characteristics of the uncertain RSC currents controlled system based on (1). The Bode diagrams are from u_{sd} to i_{rd} considering system uncertainties listed in Table II. The curves marked with '*' are obtained with the nominal model with $slip$=0.2 and K_{sc}=50%, and the other curves are for the uncertain models with different parameter perturbation. The plots of uncertain models represent sampled values of the system parameters within that interval. It is seen that the frequency characteristics of i_{rd} have a range of variations with different wind speed, SC level and grid reactance. It is also seen the sub-synchronous resonance frequency of rotor currents vary with different uncertain parameters.

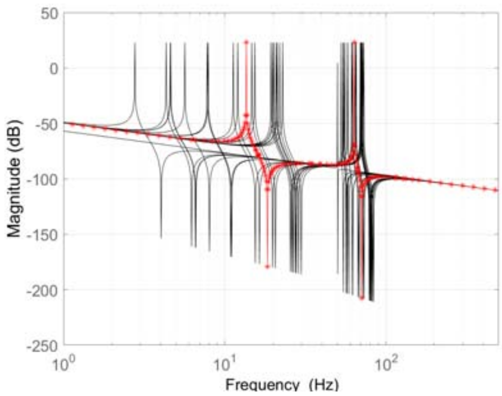

a. Bode plots with uncertain Ksc between 0 and 100%

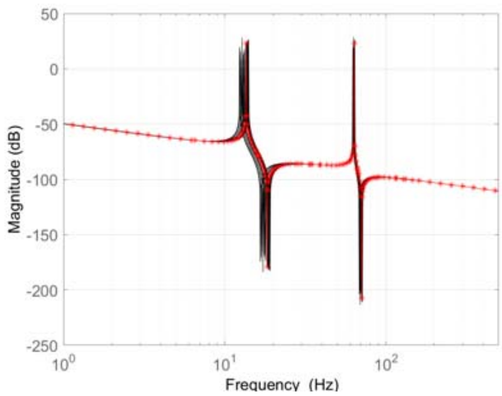

b. Bode plots with uncertain $slip$ of [-0.3, 0.3]

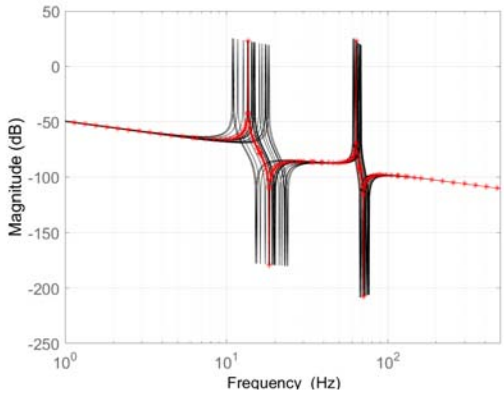

c. Bode plots with uncertain system reactance between 50% and 150%

Fig. 2. Bode plots of the uncertain system model

Fig. 3 shows the eigenvalue loci when the $slip$ increases from -0.3 to 0.3 in which the starting point is marked with '*' and the ending point is marked with 'o'. By Comparing Fig. 3a and Fig. 3b, it is seen that there are three basic natural oscillation modes after series compensation, which are the rotor currents mode $slip \times fs$, super-synchronous mode and sub-synchronous mode. Define the electrical resonance frequency as,

$$f_n = f_s \sqrt{\frac{X_{sc}}{X_{L_\Sigma}}} \tag{4}$$

where $X_{L\sum}$ is the whole system equivalent reactance, described as $L_{LT}+L_{ls}+L_{lr}$ [1]. It is seen from Fig. 3 the super-synchronous frequency and the sub-synchronous frequency are $fs + fn$ and $fs - fn$, respectively. fn is approximately 23 Hz with the K_{sc} is 50%. With the *slip* increases, the eigenvalues of the sub-synchronous mode have moved from the left half panel to the right half panel which makes the system unstable. The eigenvalues analysis result is similar with the series capacitor varies [12], [13].

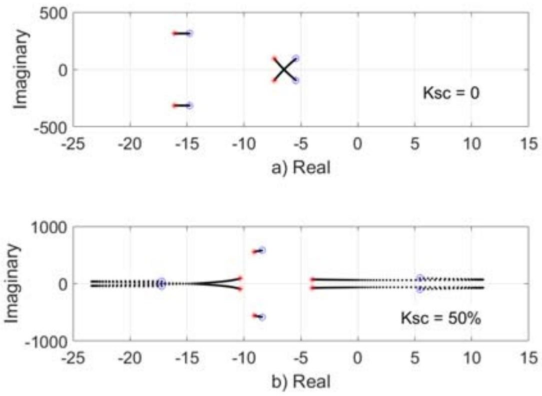

Fig. 3. Eigenvalue loci of the open-loop system with *slip* from -0.3 (marked as '*') to 0.3 (marked as 'o')

The conventional RSC currents controller uses the PI regulator, which can be described by the transfer function as,

$$\mathbf{u} = (k_p + \frac{k_i}{S})(\mathbf{r} - \mathbf{y}) \tag{5}$$

where $\boldsymbol{r}=[i_{rd}^*, i_{rq}^*]$ is the reference vector of the rotor currents controller. Synthesizing (5) with (1), the closed-loop system eigenvalue loci is obtained and shown in Fig. 4.

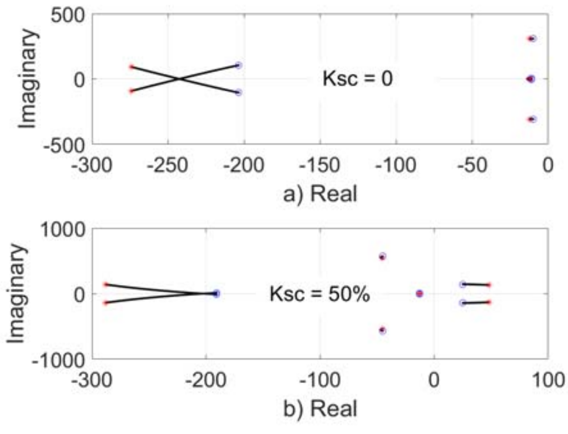

Fig. 4. Eigenvalue loci of the closed-loop system with *slip* from -0.3 to 0.3

It is seen that the PI rotor current controller makes the sub-synchronous mode located at the right half plane within the whole range of the *slip*. Compared with Fig. 3, the SSCI is more severe because the PI controller is involved. The PI current controller worsens the stability of the whole system.

2.3. SSCI Damping Control Requirements

Based on the above SSCI analysis, the sub-synchronous oscillation frequency is $f_s - f_n$. The SSCI induces the sub-synchronous oscillation of the rotor currents with the frequency of $|f_n - f_r|$ at the synchronously rotating *dq* frame. The sub-synchronous oscillation components of the currents shall be damped and the currents are with a low *THD* as the SC level changing from 0 to 1.

Considering the switching frequency of the PWM converters is usually *1 kHz to 5 kHz*, the acceptable bandwidth frequency of the SSCI damping controller shall not be less than *300 Hz* in order to guarantee the system dynamic performance.

It is also noticed the above uncertainties greatly influence the oscillation currents during the SSCI. Therefore, the SSCI damping controller must guarantee enough system robustness, including the RS and RP.

3. H∞ SSCI Controller Design

3.1. H∞ Controller Structure Design

Fig. 5 shows the control structure of the RSC in the *dq* synchronously rotating coordinates. *K* is the rotor current damping controller which is designed based on the H∞ control method. The reference signal of *K* is derived by the PQ power loop, and the measurement signal of *K* is the *dq* rotor currents.

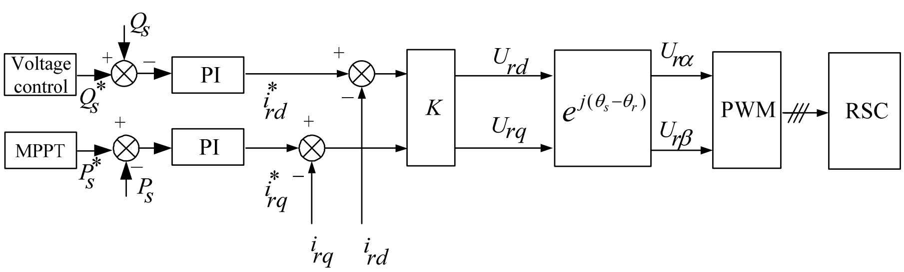

Fig. 5. Control structure diagram of RSC with *K*

The control configuration of *K* for the H∞ synthesis is shown in Fig. 6, which is based on the theory of the mixed sensitivity H∞ control and the signal based H∞ control [28]. The design of the S/KS mixed sensitivity minimization in a standard form for tracking performance and the weight to describe the multiplicative dynamic model uncertainty is adopt. The system state-space model G is divided into the state-space representation of the plant and the state-space representation of the disturbances, denoted as G_s (A, B_1, C, D) and G_d (A, B_2, C, D), respectively. The uncertain parameters in Table II can be represented in the frequency domain using unstructured multiplicative output uncertainties, marked as Δ. Δ is any stable transfer function which is less than 1 in magnitude at each frequency, representing all the uncertainties and satisfying $\|\Delta\|_\infty \leq 1$ [28]. As such, G can be described as $G_p=(1+W_o\Delta)G_N$ where G_P is the uncertain model, and G_N is the nominal model. W_o is a rational transfer function weight to cover the set of G_p. The input vector of Δ is marked as $\boldsymbol{y}_\Delta$ and the output vector of Δ is marked as $\boldsymbol{u}_\Delta$. The SSCI controller is marked as K. The input of K is $\boldsymbol{r}$-$\boldsymbol{y}$=$[i_{rd}^*-i_{rd}, i_{rq}^*-i_{rq}]$ and marked as $\boldsymbol{v}$. Regarding $\boldsymbol{r}$ as an external disturbance, the external disturbance vector can be described as $\boldsymbol{w}$=[$\boldsymbol{r}$,$\boldsymbol{d}$].

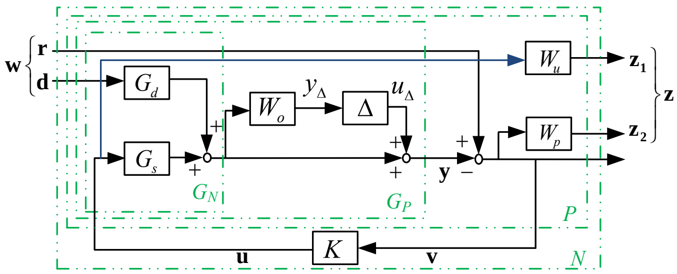

Fig. 6. The control configuration for H∞ synthesis

It is seen there are three weighting functions in Fig. 6. $\boldsymbol{u}$ and $\boldsymbol{v}$ are shaped along with weighting functions W_u and W_p , respectively. $\boldsymbol{z}$=[z_1, z_2] is the weight controlled output. W_o is another weighting function as an uncertainty filter. The block with G_s, G_d, W_o, W_u and W_p is a shaped generalized plant model and marked as P. The block N consists of P and K. So the state-space representation of P can be derived as (6).

$$\begin{bmatrix} y_\Delta \\ z \\ v \end{bmatrix} = P(s)\begin{bmatrix} u_\Delta \\ w \\ u \end{bmatrix} = \begin{bmatrix} P_{11}(s) & P_{12}(s) \\ P_{21}(s) & P_{22}(s) \end{bmatrix}\begin{bmatrix} u_\Delta \\ w \\ u \end{bmatrix}$$
$$= \left[\begin{array}{ccc|c} 0 & 0 & G_dW_o & G_sW_o \\ 0 & 0 & 0 & W_u \\ -W_p & W_p & -W_pG_d & -W_pG_s \\ \hline -I & I & -G_d & -G_s \end{array}\right]\begin{bmatrix} u\Delta \\ w \\ u \end{bmatrix} \tag{6}$$

Define the system sensitivity function as $S=(I+G_sK)^{-1}$. The state-space representation of N can be represented through the linear fractional transformation (LFT) between P and K as (7).

$$N = P_{11} + P_{12}K(I - P_{22}K)^{-1}P_{21} \overset{\Delta}{=} F_l(P,K)$$
$$= \begin{bmatrix} -G_sW_oKS & G_sW_oKS & G_dW_o - G_sW_oKSG_d \\ -W_uKS & W_uKS & -W_uKSG_d \\ W_p(G_sKS - I) & W_p(I - G_sKS) & W_p(G_sKS - I)G_d \end{bmatrix} \tag{7}$$

The design of the H$_\infty$ optimal controller is to find a stabilizing function K to minimize the largest gain for any input direction from $\boldsymbol{w}$ to $\boldsymbol{z}$, which is the peak of the singular value of the closed-loop transfer function $N(s)$, and can be described by an H$_\infty$ norm as (8).

$$\|N\|_\infty = \max_\omega \bar{\delta}(N(j\omega)) = \gamma_{\min} < \gamma \tag{8}$$

The optimal solution of (8) is marked as $\gamma_{\min}$, which can be obtained by solving the standard two-Riccati formula [25]. The γ-iteration algorithm is adopted which defines a proper value $\gamma \geq \gamma_{\min}$ to approach the optimal value $\gamma_{\min}$, as an H$_\infty$ suboptimal problem. For a nominal system, γ can be set as 1.

3.2. Weighting Function Design

The perturbation of G_p due to the uncertainties can be measured in terms of the maximum singular value $\bar{\sigma}$. Therefore, if $\bar{\sigma}(W_oG_N) \geq \bar{\sigma}(G_P - G_N)$, all the possibilities of G_p can be included in $(1+ W_o\Delta)G_N$. A simple first order filter is used as,

$$W_o = \frac{\tau s + \gamma_o}{(\tau / \gamma_\infty)s + 1} \tag{9}$$

where the relative uncertainty at steady state is γ_o. $1/\tau$ is the frequency at which the relative uncertainty reaches about 100%. γ_∞ is the magnitude of the weight at high frequency. Fig. 7 shows the singular value curves of G_p-G_N and W_oG_N, showing that the curve of $\sigma(W_oG_N)$ can cover majority possible curves of $\sigma(G_P$-$G_N)$. The uncertainty of G_P is defined as a parameter interval based on Table II. The Bode plots represent randomly sampled values of the system parameters within that interval. It is noticed the two oscillation frequencies of $\sigma(G_P$-$G_N)$ vary in a wide range and W_o adopts a simple first order expression, $\sigma(W_oG_N)$ cannot cover all the values of $\sigma(G_P$-$G_N)$ at the oscillation frequencies. The overall robustness of the system can be further guaranteed by other weighting functions. It is seen from Fig. 7 that W_u can limit the controller output gain. Therefore, it influences the bandwidth. For a normalized system, a reasonable range of W_u is,

$$W_u \leq 1 \tag{10}$$

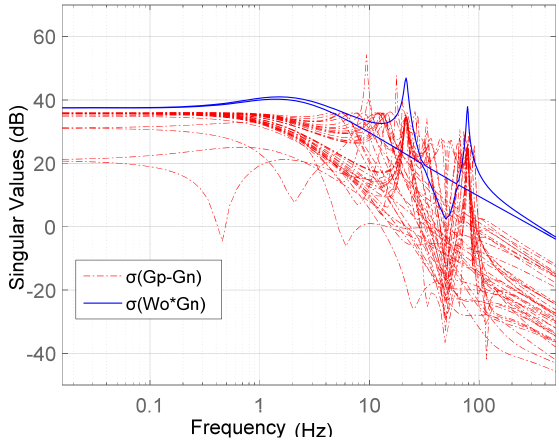

Fig. 7. The singular value curves of W_oG_N and G_P-G_N

Wp is designed to guarantee the tracking performance of the controller to the fundamental. A low pass filter is designed to shape the low frequency characteristic of the controller as,

$$W_p = \frac{s / M + \omega_1}{s + \omega_1 A} \tag{11}$$

where the low-frequency gain of $1/|W_p(j\omega)|$ is A, the high-frequency gain is M, and the asymptote of the amplitude-frequency curve crosses 1 at ω_1. Fig. 8 shows the singular values of the uncertain closed-loop system, marked as T. It is seen all the amplitude-frequency curves of T are below the curve of $1/W_o$ with the bandwidth frequencies above 400 Hz, satisfying the control requirements.

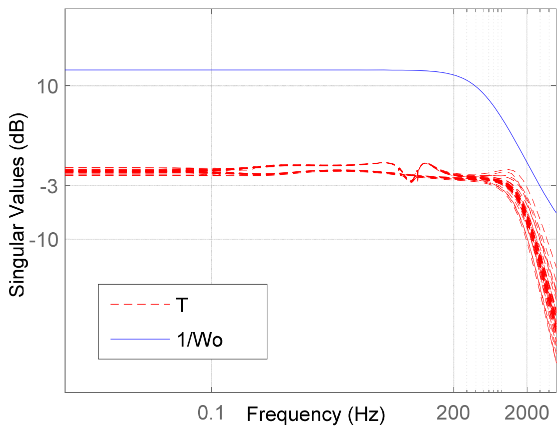

Fig. 8. The singular value curves of $1/W_o$ and T

3.3. Robust Stability Validation

The structured singular value $\mu(M)$ provides a way to assess the stability and performance of a MIMO system under a class of norm-bounded structured perturbations. With all the uncertainties nominally structured into Δ, the system *NΔ*-structure in Fig. 6 can be rearranged as a *MΔ*-structure in Fig. 9, in which $M=N_{11}$. Based on this, the criteria of the RS and RP can be derived by $\mu(M)$ in (12), which is obtained by the DK iteration [27]-[28].

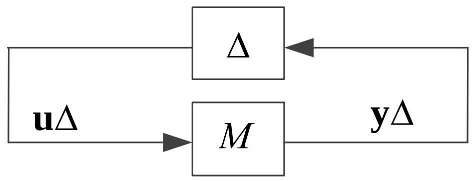

Fig. 9. *N-Δ* structure diagram for RP analysis

$$\begin{cases} RS \Leftrightarrow \mu_{\Delta}(N_{11}) < 1, \forall \omega \\ RP \Leftrightarrow \mu_{\hat{\Delta}}(N) < 1, \forall \omega, \hat{\Delta} = \begin{bmatrix} \Delta & 0 \\ 0 & \Delta_p \end{bmatrix} \end{cases} \tag{12}$$

The parameters of K are tuned to satisfy both the H_∞ suboptimal bound in (8) and the RS and RP bounds in (12). The controller parameters are listed in Table III. Using the Matlab-Robust control toolbox with the μ-toolbox, the order of K is reduced to 6 through the Hankel minimum degree approximation (MDA). The γ value is 0.92, satisfying the requirement in (8). The μ-curves of the RS and RP are shown in Fig. 10 and Fig. 11. It is seen the frequencies of the two peaks in Fig. 11 correspond to the super-synchronous mode and the sub-synchronous mode. All the values of μ are below 1(abs), satisfying the RS and RP requirements in (12).

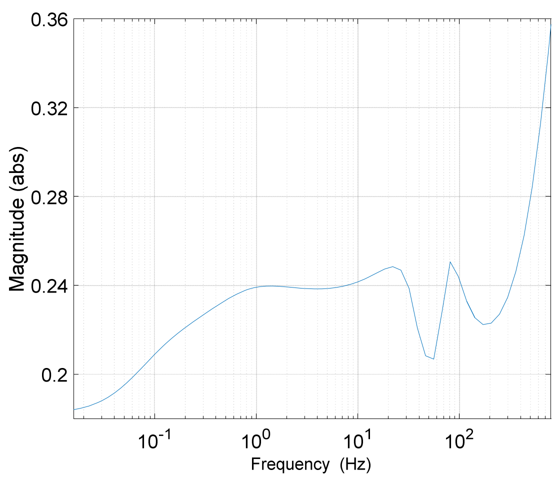

Fig. 10. The μ-curves for RS

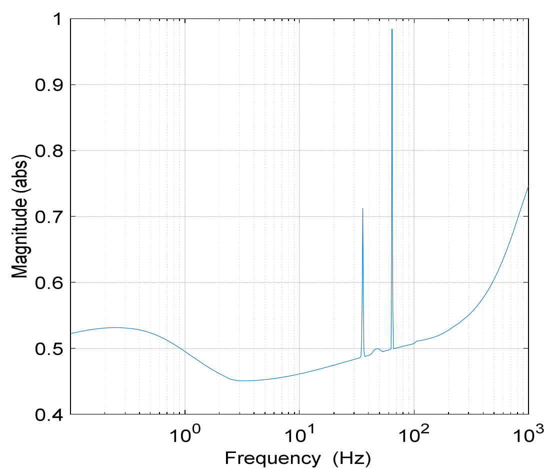

Fig. 11. The μ-curves for RP

Table III

Parameters of the weighting functions

γ_∞	τ	γ_o	M	A	ω_1	W_u
4	$\frac{1}{1.25\times10^4}$	4	0.8	15	800π	0.5

Fig. 12a shows the eigenvalue loci of the system based on the H∞ damping control when the *slip* increases from -0.3 to 0.3. The starting point is marked with '*' and the ending point is marked with 'o'. Fig. 12b shows the eigenvalue loci when the system reactance increases from 50% to 150%. It is seen from the zoomed part of the plot in Fig. 12, all eigenvalues near the origin are located at the left half plane. Compared with Fig. 4b, the unstable sub-synchronous mode of the system has been corrected to be the stable region through the H∞ damping control.

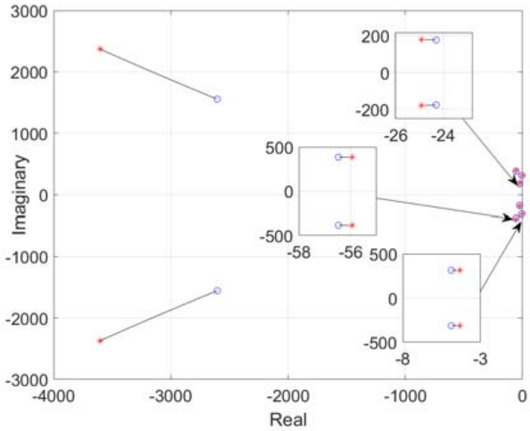

a) Eigenvalue loci of H∞ control with *slip* from -0.3 (marked with '*') to 0.3 (marked with 'o'), K_{sc}=50%

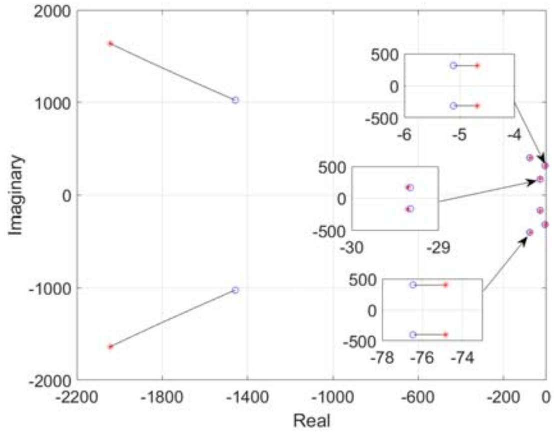

b) Eigenvalue loci of H∞ control with L_{LT} from 50% (marked with '*') to 150% (marked with 'o'), K_{sc}=50%

Fig. 12. Eigenvalue loci of closed-loop system with different uncertainties

4. Case study

Case studies were performed using Matlab / Simulink with a 90 MW DFIG based WF to verify the SSCI damping performance of the H_∞ current controller. The reactive power reference was set as 0. The grid system structure is shown in Fig.13. The PI regulator of the RSC current control loop paralleled with a SSCI damping filter, named as the damp control in this paper, was simulated to compare with the H_∞ damping controller. The transfer function of the damp control filter is (13), and the parameters of the PI controller and SSCI damping filter are designed based on [20] and listed in Table IV.C.

$$G_{damp-filter} = \frac{1+T_1 s}{1+T_2 s} \tag{13}$$

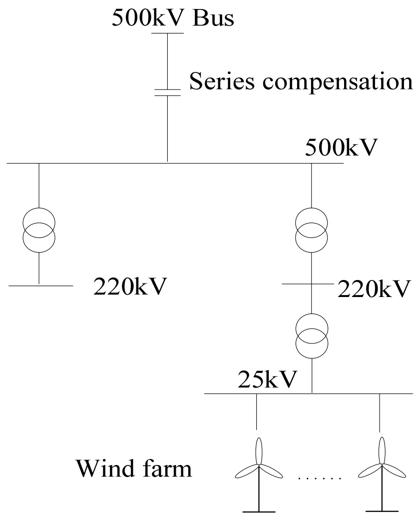

Fig. 13. The grid system structure of the studied model

4.1. Performance with different SC levels

Fig. 14 compares the rotor currents with the H_∞ damping control (Hinf) and PI control with and without the damping filter at two SC levels (PI and Damp). The series capacitor is added at 10s with K_{sc} being from 0 to 5% and 25%, respectively. R_L and L_{LT} are all nominal value, and the wind speed is 6 m/s. It is shown that i_{rd} with the PI control has obvious sub-synchronous oscillation both with K_{sc} being 5% and 25%. The sub-synchronous oscillation of rotor currents with the damping filter can be mitigated when K_{sc} is 5%. However, with K_{sc} increased to 25%, the sub-synchronous oscillation of rotor currents cannot be well mitigated. The H_∞ control still shows good performance with K_{sc} increased to both 5% and 25%.

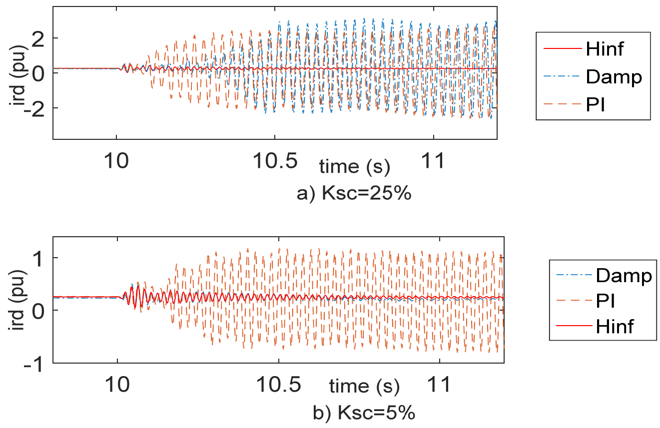

Fig. 14. Rotor current comparison with different SC level

It is seen from Fig. 15 that the sub-synchronous oscillations of the rotor currents, stator currents and output power can be well mitigated by the H$_\infty$ damping control with K_{sc} increased to 25%. The THD of stator currents between 10.2 s to 10.4 s is 1.5% with the H$_\infty$ damping control, satisfying the control requirement.

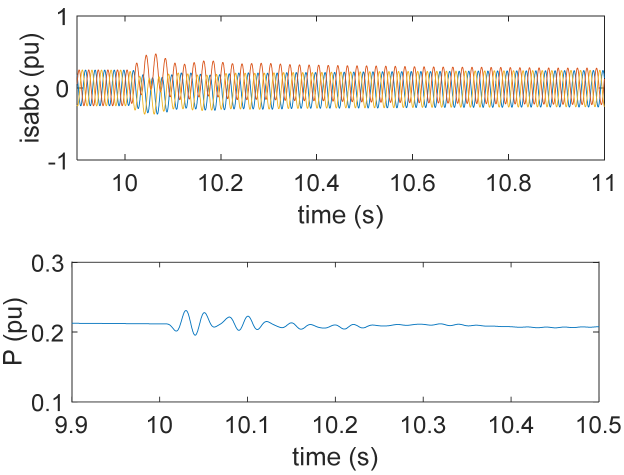

Fig. 15. Results by H$_\infty$ control with K_{sc} increasing to 25% at 10s

4.2. Performance with different wind speed

Fig. 16 shows the results with the PI, damping filter and H$_\infty$ damping control with low (6m/s) and high wind speed (12m/s). The series capacitor is added with K_{sc} being from 0 to 25% at 10s. The system parameters are all nominal values.

It is seen that rotor currents show obvious sub-synchronous oscillation both at the wind speed being 12m/s and 6m/s with the PI control. With the damping filter, the sub-synchronous oscillation of rotor currents can be mitigated at the wind speed being 12m/s. However, when the wind speed decreases to 6m/s, the sub-synchronous oscillation of rotor currents cannot be mitigated. The H$_\infty$

control can mitigate the sub-synchronous oscillation of rotor currents both at high and low wind speeds.

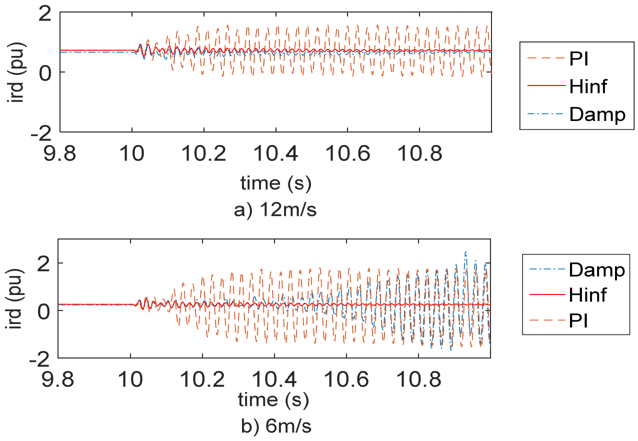

Fig. 16. Rotor currents comparison with different wind speed

4.3 Performance with system reactance disturbance

Fig. 17 shows the results with the disturbance of the system reactance up to 1.3 pu of the nominal value. The wind speed is 6 m/s. The series capacitor is added at 10s with *Ksc* increasing from 0 to 5%. It is seen that, with system reactance disturbance, the sub-synchronous oscillation of rotor currents with the damping filter can no longer be mitigated when *Ksc* is 5%, compared with Fig.14b. The H∞ controller still shows good SSO damping performance with the system parameter perturbation. The robustness of the DFIG based wind turbine with the SC compensated grid is improved by the H_∞ damping controller, compared with the damping filter.

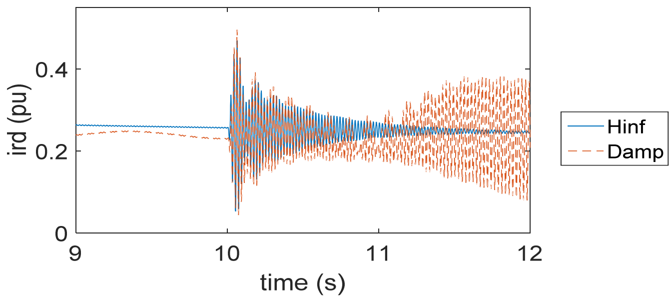

Fig. 17. Rotor currents with system reactance disturbance

4.4 Performance with grid voltage disturbance

Fig. 18 further compares the results with grid voltage fault disturbance. A three phase to ground voltage fault with 50% dip depth occurred from 10s to 10.5s. The SC level is 25% and the wind speed is 12m/s. It is seen both i_r and U_{dc} are stable with the H_∞ damping control after a dynamic process. However, the sub-synchronous oscillation is excited with the damping filter control during and after the grid fault.

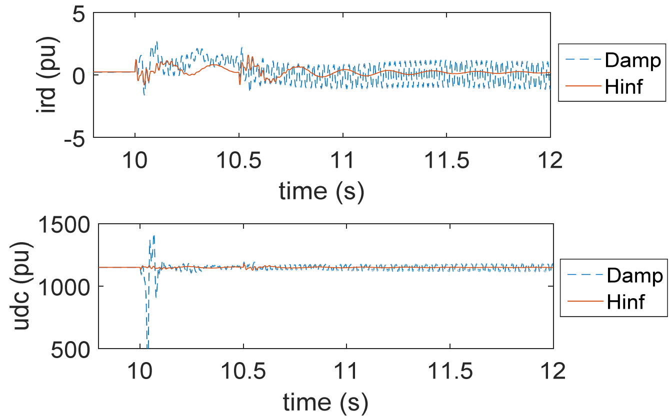

Fig. 18. Rotor currents and DC voltage under grid dip fault

A three phase to ground voltage fault with 100% dip depth occurred from 10s to 10.2s is shown in Fig. 19. It is seen, under the most severe grid voltage disturbance, the H_∞ damping control can still mitigate the sub-synchronous oscillation of rotor currents and stator currents after the fault ends. It is seen that, about 300ms dynamic regulation after the grid fault ends, the system keeps stable operation, showing good large-signal stability of the designed H_∞ damping controller.

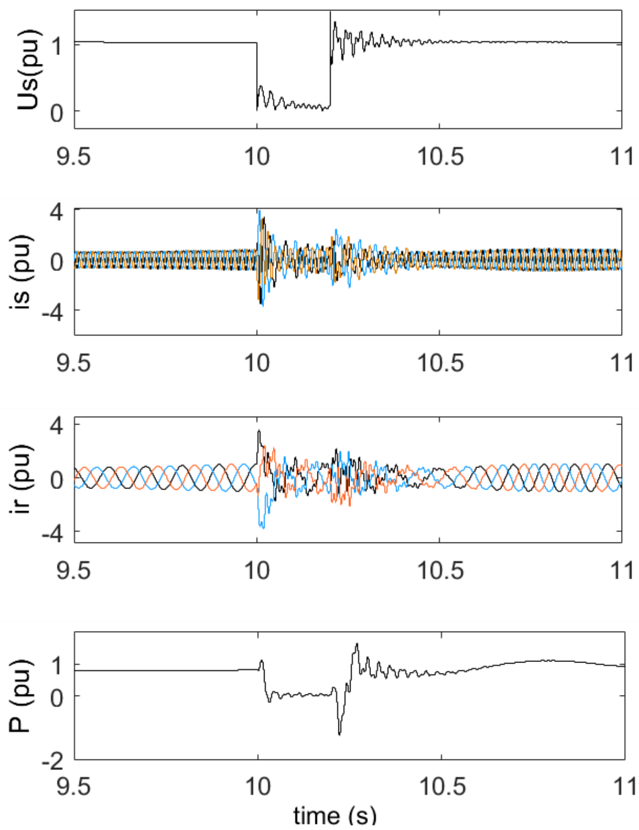

Fig. 19. H_∞ damping control performance under 100% voltage dip fault

4.5 Case study with 70% SC level

The H_∞ control performance is further studied with low wind speed, high SC level and none-nominal DFIG parameters. The wind speed is 6 m/s, the SC level changes from 0% to 70% at 10s and the system reactance is 1.3 pu of the nominal value. According to the SSCI analysis in section II, under such a low wind speed and a high SC level, the system stability shows worse performance. It is seen from Fig. 20, although the dynamic performance is worse (i.e., more severe overshoot, longer dynamic duration), the sub-synchronous oscillation of currents and output power can still be mitigated by the H_∞ damping control.

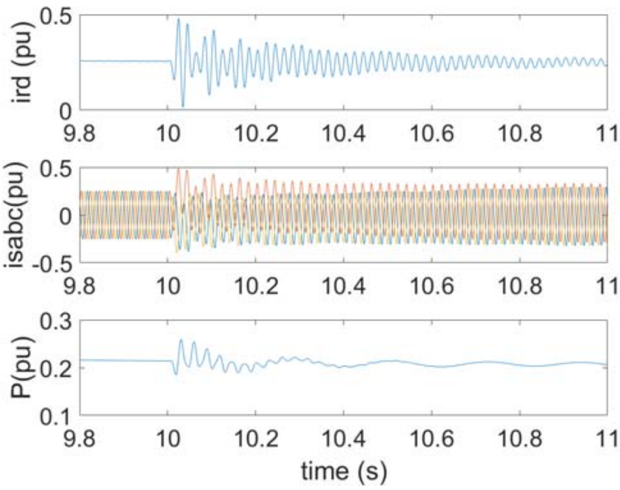

Fig. 20. Performance of the system with H_∞ controller

5. Conclusion

In this paper, a H_∞ damping controller is proposed to effectively mitigate the sub-synchronous oscillation currents due to the SSCI between the DFIG based WF and the series compensated grid lines. The developed uncertain state-space model can well reflect the main SSCI characteristics as the wind speed, SC level and grid parameters change. The designed H_∞ damping controller not only satisfies good performance of mitigating sub-synchronous oscillation currents with a low THD, but also shows enough closed-loop system bandwidth. Furthermore, the designed H_∞ damping controller guarantees robustness which is demonstrated by the μ analysis, eigenvalue analysis and time domain simulation. The H_∞ damping controller shows satisfying SSCI mitigation performance with low wind speed, high SC level and uncertain system parameter.

Appendix

The 4th DFIG model in a synchronous reference frame can be written in terms of the currents as shown in (14). In the synchronous reference frame, the dynamics of the series compensated system can be described by (15). The dynamics of the capacitor in the dc link between RSC and GSC are described by (16). The mechanical model is a two mass system described by (17).

$$\frac{d}{dt}\begin{bmatrix} i_{sd} \\ i_{sq} \\ i_{rd} \\ i_{rq} \end{bmatrix} = \frac{\omega_B}{L_m^2 - L_r L_s}\begin{bmatrix} L_r R_s & L_m^2\omega_{slip} - L_s L_r \omega_s & -L_m R_r & -L_m L_r \omega_r \\ L_s L_r \omega_s - L_m^2 \omega_{slip} & L_r R_s & L_m L_r \omega_r & -L_m R_r \\ -L_m R_s & L_s L_m \omega_r & L_s R_r & L_m^2 \omega_s - L_s L_r \omega_{slip} \\ -L_s L_m \omega_r & -L_m R_s & L_s L_r \omega_{slip} - L_m^2 \omega_s & L_s R_r \end{bmatrix}\begin{bmatrix} i_{sd} \\ i_{sq} \\ i_{rd} \\ i_{rq} \end{bmatrix} + \frac{\omega_B}{L_m^2 - L_r L_s}\begin{bmatrix} L_m & 0 & -L_r & 0 \\ 0 & L_m & 0 & -L_r \\ -L_s & 0 & L_m & 0 \\ 0 & -L_s & 0 & L_m \end{bmatrix}\begin{bmatrix} u_{rd} \\ u_{rq} \\ u_{sd} \\ u_{sq} \end{bmatrix} \quad (14)$$

$$\frac{d}{dt}\begin{bmatrix} u_{cd} \\ u_{cq} \\ i_{lq} \\ i_{ld} \end{bmatrix} = \omega_B \begin{bmatrix} 0 & -\omega_s & X_{sc} & 0 \\ \omega_s & 0 & 0 & X_{sc} \\ -1/X_{LT} & 0 & -R_L/X_{LT} & -\omega_s \\ 0 & -1/X_{LT} & \omega_s & -R_L/X_{LT} \end{bmatrix}\begin{bmatrix} u_{cd} \\ u_{cq} \\ i_{lq} \\ i_{ld} \end{bmatrix} + \omega_B \begin{bmatrix} 0 \\ 0 \\ \frac{u_{sq} - E_{gq}}{X_{LT}} \\ \frac{u_{sd} - E_{gd}}{X_L} \end{bmatrix} \quad (15)$$

$$Cu_{dc}\frac{du_{dc}}{dt} = P_r - P_g = \frac{1}{2}(u_{rd}i_{rd} + u_{rq}i_{rq}) - \frac{1}{2}(u_{gd}i_{gd} + u_{gq}i_{gq}) \quad (16)$$

$$\frac{d}{dt}\begin{bmatrix} \Delta\omega_t \\ \Delta\omega_r \\ T_g \end{bmatrix} = \omega_B \begin{bmatrix} \frac{-D_t - D_{tg}}{2H_t} & \frac{D_{tg}}{2H_t} & \frac{-1}{2H_t} \\ \frac{D_{tg}}{2H_g} & \frac{-D_t - D_{tg}}{2H_g} & \frac{1}{2H_g} \\ K_{tg}\omega_e & -K_{tg}\omega_e & 0 \end{bmatrix}\begin{bmatrix} \Delta\omega_t \\ \Delta\omega_r \\ T_g \end{bmatrix} + \begin{bmatrix} \frac{D_{tg}}{2H_t} \\ \frac{-T_e}{2H_g} \\ 0 \end{bmatrix} \quad (17)$$

TABLE IV

a. Parameters of the grid (equivalent value)

Base MVA	90 MW
Transformer inductance	0.14 pu
Transmis. line resistance	0.023 pu (12Ω)
Transmis. line inductance	0.46 pu
Series capacitor reactance	124 Ω (at 50%SC level)
Series compensation C	26 µF (at 50% SC level)
Line length	30 kilo meters

b. Parameters of the WT and WF

Rated power	1.5 MW	90 MW
Rated voltage (Line-Line)	0.69 kV	0.69 kV
Electrical base frequency	50 Hz	50 Hz
Stator resistance	0.023 pu	0.023 pu
Rotor resistance	0.016 pu	0.016 pu
Stator leakage inductance	0.18 pu	0.18 pu
Rotor leakage inductance	0.16 pu	0.16 pu
Mutual inductance	2.9 pu	2.9 pu

c. Parameters of converter controllers

DC bus voltage regulator gains	[K_P K_i]	[8 400]

GSC currents regulator gains	[K_P K_i]	[0.83 5]
Speed regulator gains	[K_P K_i]	[3 0.6]
RSC currents regulator gains	[K_P K_i]	[0.2 8]
Q and P regulator gains	[K_P K_i]	[0.05 20]
SSCI damping filter	[T_1 T_2]	[0.2 0.002]

Acknowledgment

This work is supported by the National Science Foundation of China (51407118).

Reference

[1] S. R. W. Group, "Terms, Definitions and Symbols for Subsynchronous Oscillations," *IEEE Trans. Power Appar. Syst.*, vol. PAS-104, no. 6, pp. 1326–1334, 1985.

[2] I. S. R. T. Force, "First benchmark model for computer simulation of subsynchronous resonance," *IEEE Trans. Power Appar. Syst.*, vol. 96, no. 5, pp. 1565–1572, Sep. 1977.

[3] L. C. Gross, "Sub-Synchronous Grid Conditions: New Event, New Problem, and New Solutions," in *Proc. 37th Annu. Western Protective Relay Conf.*, 2010, pp. 1–19.

[4] "Second Benchmark Model for Computer Simulation of Subsynchronous Resonance," *IEEE Trans. Power Appar. Syst.*, vol. PAS-104, no. 5, pp. 1057–1066, 1985.

[5] H. A. Mohammadpour and E. Santi, "Sub-synchronous resonance analysis in DFIG-based wind farms: Definitions and problem identification — Part I," in *2014 IEEE Energy Conversion Congress and Exposition (ECCE)*, 2014, pp. 812–819.

[6] Yun Wang, Qiuwei Wu, and Shaoli Kang, "Sub-synchronous interaction analysis between DFIG based wind farm and series compensated network," in *2016 IEEE PES Asia-Pacific Power and Energy Engineering Conference (APPEEC)*, 2016, pp. 359–363.

[7] A. Ostadi, A. Yazdani, and R. K. Varma, "Modeling and Stability Analysis of a DFIG-Based Wind-Power Generator Interfaced With a Series-Compensated Line," *IEEE Trans. Power Deliv.*, vol. 24, no. 3, pp. 1504–1514, Jul. 2009.

[8] M. Sahni, Y. Cheng, and Y. Zhou, "Sub-synchronous interaction in Wind Power Plants- part II: An ercot case study," in *2012 IEEE Power and Energy Society General Meeting*, 2012, pp. 1–9.

[9] B. Badrzadeh, M. Sahni, D. Muthumuni, and A. Gole, "General methodology for analysis of sub-synchronous interaction in wind power plants," in *2013 IEEE Power & Energy Society General Meeting*, 2013, pp. 1–1.

[10] H. A. Mohammadpour and E. Santi, "Sub-synchronous resonance analysis in DFIG-based wind farms: Mitigation methods — TCSC, GCSC, and DFIG controllers — Part II," in *2014 IEEE Energy Conversion Congress and Exposition (ECCE)*, 2014, pp. 1550–1557.

[11] L. Wang, X. Xie, Q. Jiang, H. Liu, Y. Li, and H. Liu, "Investigation of SSR in Practical DFIG-Based Wind Farms Connected to a Series-Compensated Power System," *IEEE Trans. Power Syst.*, vol. 30, no. 5, pp. 2772–2779, Sep. 2015.

[12] L. Fan, R. Kavasseri, Z. L. Miao, and C. Zhu, "Modeling of DFIG-Based Wind Farms for SSR Analysis," *IEEE Trans. Power Deliv.*, vol. 25, no. 4, pp. 2073–2082, Oct. 2010.

[13] L. Fan, C. Zhu, Z. Miao, and M. Hu, "Modal Analysis of a DFIG-Based Wind Farm Interfaced With a Series Compensated Network," *IEEE Trans. Energy Convers.*, vol. 26, no. 4, pp. 1010–1020, Dec. 2011.

[14] K. Narendra *et al.*, "New microprocessor based relay to monitor and protect power systems against sub-harmonics," in *2011 IEEE Electrical Power and Energy Conference*, 2011, pp. 438–443.

[15] Z. Miao, "Impedance-Model-Based SSR Analysis for Type 3 Wind Generator and Series-Compensated Network," *IEEE Trans. Energy Convers.*, vol. 27, no. 4, pp. 984–991, Dec. 2012.

[16] H. A. Mohammadpour and E. Santi, "Optimal adaptive sub-synchronous resonance damping controller for a series-compensated doubly-fed induction generator-based wind farm," *IET Renew. Power Gener.*, vol. 9, no. 6, pp. 669–681, Aug. 2015.

[17] H. Ghasemi, G. B. Gharehpetian, S. A. Nabavi-Niaki, and J. Aghaei, "Overview of subsynchronous resonance analysis and control in wind turbines," *Renew. Sustain. Energy Rev.*, vol. 27, pp. 234–243, Nov. 2013.

[18] S. Muller, M. Deicke, and R. W. De Doncker, "Doubly fed induction generator systems for wind turbines," *IEEE Ind. Appl. Mag.*, vol. 8, no. 3, pp. 26–33, 2002.

[19] R. Pena, J. C. Clare, and G. M. Asher, "Doubly fed induction generator using back-to-back PWM converters and its application to variable-speed wind-energy generation," *IEE Proc. - Electr. Power Appl.*, vol. 143, no. 3, p. 231, 1996.

[20] G. D. Irwin, A. K. Jindal, and A. L. Isaacs, "Sub-synchronous control interactions between type 3 wind turbines and series compensated AC transmission systems," in *2011 IEEE Power and Energy Society General Meeting*, 2011, pp. 1–6.

[21] P.-H. Huang, M. S. El Moursi, W. Xiao, and J. L. Kirtley, "Subsynchronous Resonance Mitigation for Series-Compensated DFIG-Based Wind Farm by Using Two-Degree-of-Freedom Control Strategy," *IEEE Trans. Power Syst.*, vol. 30, no. 3, pp. 1442–1454, May 2015.

[22] M. P. S. Gryning, Q. Wu, M. Blanke, H. H. Niemann, and K. P. H. Andersen, "Wind Turbine Inverter Robust Loop-Shaping Control Subject to Grid Interaction Effects," *IEEE Trans. Sustain. Energy*, vol. 7, no. 1, pp. 41–50, Jan. 2016.

[23] Y. W. Li, D. M. Vilathgamuwa, F. Blaabjerg, and P. C. Loh, "A robust control scheme for medium-voltage-level DVR implementation," *IEEE Trans. Ind. Electron.*, vol. 54, no. 4, pp. 2249–2261, 2007.

[24] G. Willmann, D. F. Coutinho, L. F. A. Pereira, and F. B. Libano, "Multiple-Loop H-Infinity Control Design for Uninterruptible Power Supplies," *IEEE Trans. Ind. Electron.*, vol. 54, no. 3, pp. 1591–1602, Jun. 2007.

[25] Y. Wang, Q. Wu, W. Gong, and M. P. S. Gryning, “H_{∞} Robust Current Control for DFIG-Based Wind Turbine Subject to Grid Voltage Distortions,” *IEEE Trans. Sustain. Energy*, vol. 8, no. 2, pp. 816–825, Apr. 2017.

[26] M. Djukanovic, M. Khammash, and V. Vittal, “Application of the structured singular value theory for robust stability and control analysis in multimachine power systems. I. Framework development,” *IEEE Trans. Power Syst.*, vol. 13, no. 4, pp. 1311–1316, 1998.

[27] J. C. Doyle, K. Glover, P. P. Khargonekar, and B. A. Francis, “State-space solutions to standard H/sub 2/ and H/sub infinity / control problems,” *IEEE Trans. Automat. Contr.*, vol. 34, no. 8, pp. 831–847, 1989.

[28] S. Skogestad and I. Postlethwaite, *Multivariable feedback control: analysis and design*, Vol. II. New York: WILEY, 2005.

[29] A. E. Leon and J. A. Solsona, “Sub-Synchronous Interaction Damping Control for DFIG Wind Turbines,” IEEE Trans. Power Syst., vol. 30, no. 1, pp. 419–428, Jan. 2015.

[30] H. Liu, X. Xie, Y. Li, H. Liu, and Y. Hu, “Mitigation of SSR by embedding subsynchronous notch filters into DFIG converter controllers,” IET Gener. Transm. Distrib., vol. 11, no. 11, pp. 2888–2896, Aug. 2017.

[31] H. Liu, L. Wang, X. Xie, and Y. Han, “Optimal design of linear subsynchronous damping controllers for stabilising torsional interactions under all possible operating conditions,” IET Gener. Transm. Distrib., vol. 9, no. 13, pp. 1652–1661, Oct. 2015.